Composites: Part A 46 (2013) 69–79

Contents lists available at SciVerse ScienceDirect

Composites: Part A

journal homepage: www.elsevier.com/locate/compositesa

Ballistic resistance of hybrid-cored sandwich plates: Numerical and experimental assessment

C.Y. Ni [a], Y.C. Li [b], F.X. Xin [a,*], F. Jin [a], T.J. Lu [a,*]

[a] State Key Laboratory for Mechanical Structure Strength and Vibration, School of Aerospace, Xi'an Jiaotong University, Xi'an 710049, China
[b] Engineering Institute of Engineering Corps, PLA University of Science and Technology, Nanjing 210007, China

ARTICLE INFO

Article history:
Received 30 March 2012
Received in revised form 2 July 2012
Accepted 12 July 2012
Available online 31 July 2012

Keywords:
A. Hybrid
B. Impact behavior
C. Finite element analysis (FEA)

ABSTRACT

The impact responses and ballistic resistance of sandwich plates having three different types of hybrid cores are investigated. The hybrid cores include metallic pyramidal lattice trusses, metallic pyramidal lattice trusses with ceramic prism insertions, and metallic pyramidal lattice trusses with ceramic prism insertions and void-filling epoxy resin. Three-dimensional (3D) finite element (FE) simulations are carried out for each sandwich type impacted by a hemispherical projectile. Upon validating the FE simulation results with experimental measurements, the ballistic limit velocity, energy absorption and failure mechanisms for each type of the sandwich as well as the influence of key material, structural and topological parameters are investigated systematically. Sandwich plates having metallic pyramidal lattice core with ceramic insertions and epoxy resin filling void spaces are found to outperform the other two sandwich types. It is also demonstrated that the back face-sheet plays a more significant role than the front face-sheet in resisting ballistic impacts.

1. Introduction

Lightweight sandwich structures with highly porous 2D (two-dimensional, usually prismatic such as honeycombs) or 3D (three-dimensional) periodic metallic lattice truss cores have multi-functional attributes, including high stiffness/strength, energy absorption, shock mitigation, heat dissipation and sound insulation [1–7], due mainly from the combined advantage of the metallic lattice core and the composite (hybrid) configuration. In particular, in recent years it has been established that sandwich structures with hybrid cores can effectively withstand ballistic impact. The present paper aims to assess, both numerically and experimentally, the ballistic responses of hybrid-cored sandwich structures having a variety of cores, including the pyramidal lattice truss core, the pyramidal-ceramic hybrid core, and the pyramidal-ceramic–epoxy hybrid core.

Extensive efforts have been devoted to investigating the impact/ballistic response and energy absorption capability of a wide range of engineering structures. For typical instance, the penetration of monolithic or layered metal sheets by a normal incidence projectile has been widely studied numerically and experimentally [8–13]. It was found that different nose shapes of the projectile significantly affect the energy absorption, the failure mode and the ballistic limit velocity of the projectile-plate system. Moreover, the ballistic performance of a double-layered shield could be improved by adjusting the strength and ductility of the two layers [10,11]. Recent work has demonstrated that porous cellular metals have excellent impact energy absorption capability, and a few periodic topologies are particularly efficient for mitigating high intensity dynamic loading such as that associated with the impingement of blast created shock waves [14–16]. In particular, Yungwirth et al. [17] demonstrated experimentally that, relative to monolithic plates of equal mass, all-metallic sandwich plates with pyramidal lattice truss cores displayed substantially higher ballistic resistance against spherical steel projectile penetration. Built upon this work, Yungwirth et al. [18] investigated experimentally the ballistic behavior of sandwich plates with hybrid cores (e.g., metallic lattice-polymer and metallic lattice-ceramic) and it was found that the hybrid core could offer huge potential for mending the ballistic properties of the sandwich. Similar hybrid or composite material concepts have been exploited to improve the energy absorption and shock mitigation capability of engineering materials/structures [19–22].

To explore further the mechanisms underlying the impact responses and ballistic resistance of novel hybrid-cored sandwich structures, numerical simulations with the method of finite elements (FE) are performed on sandwich plates with three different types of core: metallic pyramidal lattice trusses, metallic pyramidal lattice trusses with ceramic prism insertions, and metallic pyramidal lattice trusses with ceramic prism insertions and void-

* Corresponding authors. Tel./fax: +86 29 8266 5937 (T.J. Lu).
E-mail addresses: fengxian.xin@gmail.com (F.X. Xin), tjlu@mail.xjtu.edu.cn (T.J. Lu).

1359-835X/$ - see front matter © 2012 Elsevier Ltd. All rights reserved.
http://dx.doi.org/10.1016/j.compositesa.2012.07.019

filling epoxy resin. Upon validating the numerical simulations with experimental measurement results obtained under hemispherical projectile impact, the ballistic limit velocity, energy absorption and failure mechanisms for each type of the sandwich as well as the influence of key material, structural and topological parameters are investigated systematically. Notice that the ballistic limit velocity is defined here as the maximum velocity at which a particular projectile is expected to consistently fail to penetrate armor of given thickness and physical properties at a specified angle of obliquity (normal penetration here). Also, whilst the experimental study presented here is fairly similar to that carried out by Yungwirth et al. [17,18], its main purpose is to provide test data (especially the ballistic resistance of Type II and III sandwiches) that can used to validate the numerical predictions. Further, the measured ballistic performance of Type II and III sandwiches under different projectile impact velocities and the role of the void-filling epoxy resin have not been reported in the open literature.

2. Problem description

Consider sandwich plates having three different core types as shown schematically in Fig. 1: (a) pyramidal metallic lattice core (Type I), (b) pyramidal metallic lattice core with ceramic prism insertions (Type II), and (c) pyramidal metallic lattice core with ceramic prism insertions and void-filling epoxy resin (Type III). The hybrid-cored sandwich plates are clamp supported and impacted by a hemispherical projectile at the plate center as illustrated in Fig. 2. The aim of the study is to investigate experimentally and numerically the impact responses of each sandwich type, compare their ballistic limit velocities, and explore the influence of key material, structural and topological parameters upon the ballistic limit velocity.

3. Numerical model

The commercially available FE package ANSYS is utilized to generate 3D meshes for each sandwich plate. The meshed model is then transferred to the explicit integration version of the FE code LS-DYNA [23] to perform numerical simulations.

3.1. Finite element model

A FE model for each type of the sandwich plate is established first using 3D reduced integration solid elements (SOLID 164). For illustration, Fig. 3 compares the FE mesh of pyramidal lattice truss core with that fabricated using the method of sheet slitting, expansion and flattening. For simplicity and to ensure the stability of numerical simulations, the slightly bent (warping) features near each joint of the actual lattice core are neglected in the FE model.

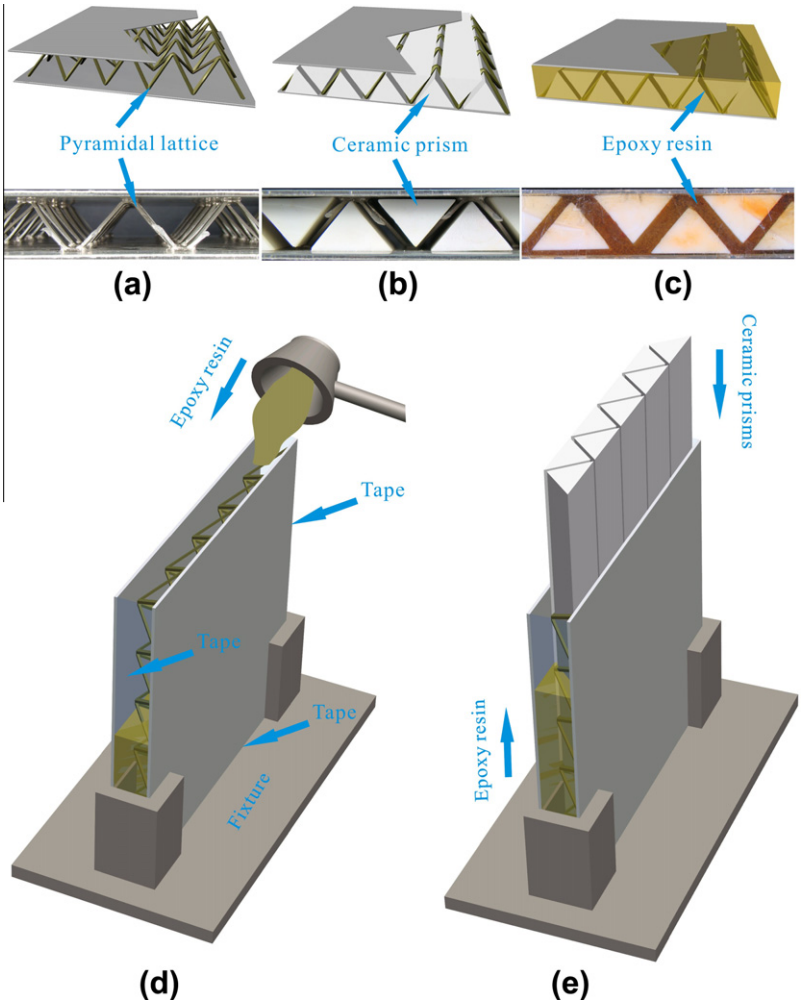

Fig. 1. Sandwich plate with: (a) pyramidal metallic lattice truss core (Type I), (b) pyramidal metallic lattice truss core with ceramic prism insertions (Type II), and (c) pyramidal metallic lattice truss core with ceramic prism insertions and void-filling epoxy resin (Type III). Assembling procedures for Type III: (d) pouring of epoxy resin into pyramidal lattice core and (e) inserting of ceramic prisms into epoxy-filled pyramidal lattice core.

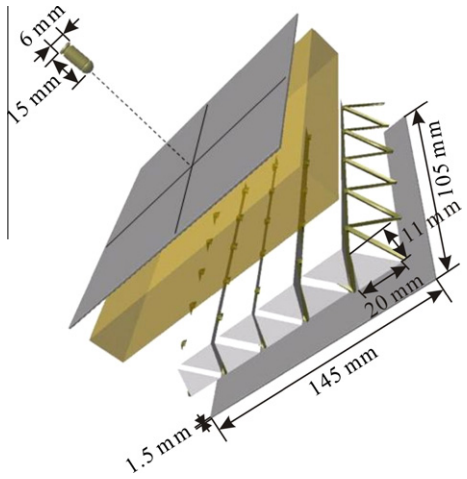

Fig. 2. Schematic of pyramidal lattice truss-cored sandwich plate with ceramic prism insertions and void-filling epoxy resin clamp supported at plate edges and impacted by a hemispherical projectile (bullet) at plate center.

The region directly under projectile impact is modeled with relatively dense meshes to highlight the penetration details.

The SOLID 164 element is defined by eight nodes having nine degrees of freedom at each node and, to save computational time and enhance reliability under large deformation conditions, the center point Gauss integration rule and hourglass control are applied. Contacts between the face-sheets and the lattice truss members are modeled as "surface to surface eroding contact", which is defined as contact surfaces that are updated once the elements on free surfaces of the structures are deleted according to material failure criteria. To simulate the mechanical performance of the bonding spots (see Fig. 3a), those between the sub-structures of the sandwich and the projectile are also modeled as "eroding contact" to emulate the penetration process. Moreover, all the contacts are defined with a scale factor of 0.5 for sliding interface penalties. Except for the void-filling epoxy that is simulated by adopting the Euler elements, all other sub-structures of the sandwich plate as well as the bullet are meshed using the Lagrange elements, with the Arbitrary Lagrangian–Eulerian (ALE) method employed to establish the FE model. To ensure the convergence of the numerical solutions, the three sandwich structures of Figs. 1 and 2 are meshed separately with 58450, 148450 and 832150 elements, and the projectile is meshed with 14000 elements, with minimum element size 0.16 mm for the projectile, 0.25 mm for pyramidal lattice truss core, 0.16 mm for central ceramic prism directly under impact, 0.52 mm for side ceramic prisms, 0.5 mm for the face-sheets, 0.48 mm for air, and 0.48 mm for epoxy resin, respectively. The selection of mesh size is a compromise between the accuracy of the numerical simulation results and the computational cost. Finer and denser elements would have resulted in a much longer calculation time than that for coarser meshes, with only a little gain in accuracy as confirmed by the mesh sensitivity analysis. Whilst the present focus is placed upon fully clamped boundary conditions, it has been established that other types of boundary constraint such as half clamped and free constraint almost have almost no influence on the impact behavior of the sandwich under the conditions as specified in Fig. 2.

3.2. Constitutive models and fracture criteria

Typically, the application of constitutive relations in the present numerical simulations includes metal explosive shaping, ballistic penetration and impact. For metallic materials under large deformation and high strain ratio, the J–C constitutive relation and fracture criterion of Johnson and Cook are known to be suitable [24]. In the current study, the face-sheets, the lattice truss core and the projectile are all modeled by applying the J–C constitutive relation and fracture criterion, with stain rate effect accounted for, and the Mie-Gruneisen equation of state model [23] is applied in conjunction with the J–C model. For the metallic material (AISI 304 stainless steel) examined here, according to the Johnson–Cook model, the yield stress σ_y is given by:

$$\sigma_y = (A + B\varepsilon_p^n)(1 + c\ln\dot{\varepsilon}^*)(1 - T^{*m}) \tag{1}$$

where A, B, m and n are material constants with B and n representing strain hardening, and ε_p is the equivalent plastic strain. Further, the fracture of a material element is defined as:

$$D = \sum \Delta\varepsilon^p / \varepsilon^f \tag{2}$$

where $\Delta\varepsilon^p$ is the increment of equivalent plastic strain and ε^f is the equivalent fracture strain for a given strain ratio, temperature, pressure and equivalent stress.

For ceramic (AD 98 alumina) prism insertions, the Johnson–Holmquist–Ceramics (JH-2) constitutive relation and fracture criterion [23] are adopted, which is particularly suitable for describing the fracture behavior of ceramics under high velocity penetration [25]. The model assumes that the strength of a ceramic is closely related with the exerting pressure, strain ratio and damage of the material, with the damage defined as the ratio of cumulative strain to failure strain and the relationship between pressure and specific heat capacity included in the volume effect of the material. The JH-2 relation reads:

$$\sigma^* = \sigma_i^* - D(\sigma_i^* - \sigma_f^*) \tag{3}$$

where σ_i^* is the intact, undamaged dimensionless effective stress, σ_f^* is the damaged dimensionless effective stress, and D is the damage parameter defined as:

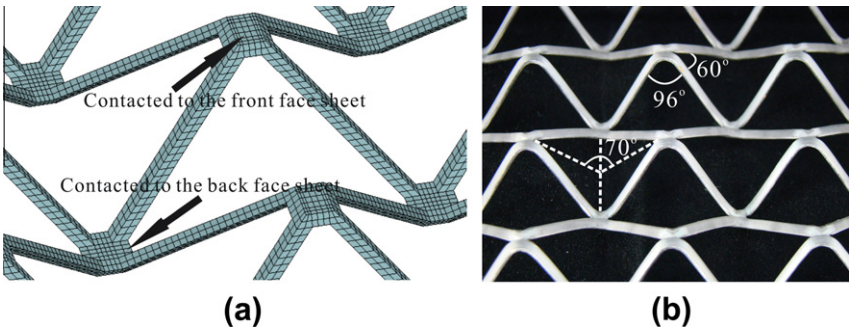

Fig. 3. Pyramidal lattice truss core: (a) finite element mesh; and (b) as fabricated.

Table 1
Material parameters for AISI 304 stainless steel used in Johnson–Cook's model and Mie-Gruneisen equation of state [27,28].

Young's modulus E (GPa)	Poisson ratio υ	Density ρ_0 (kg/m^3)	A (MPa)	B (MPa)	n	c	m
200	0.3	7900	310	1000	0.65	0.07	1.00
Slope of the shock velocity-particle velocity curve S			Gruneisen coefficient γ_0		Elastic wave speed C_0 (m/s)		
$S_1 = 1.49$, $S_2 = S_3 = 0$			1.93		4519		

Table 2
Material properties and Johnson–Holmquist–Ceramics (JH-2) parameters for AD 98 alumina used in the numerical analysis [25].

Shear modulus G (GPa)	Density ρ_0 (kg/m^3)	Hugoniot elastic limit HEL (GPa)		a	n	c
151.96	3890	6.57	0.88	0.64	0.07	
b	m	d_1	d_2	k_1 (GPa)	k_2 GPa)	k_3 (GPa)
0.28	0.6	0.01	0.7	231	−160	2374

$$D = \sum \Delta\varepsilon_p / \varepsilon_p^f \tag{4}$$

Here, $\Delta\varepsilon_p$ represents an integration cycle of the material plastic strain and ε_p^f is the material breaking strain.

Due to the low strength of the void-filling epoxy compared with either steel or ceramic, it is regarded here as a kind of hydrodynamic material and modeled by applying the Elastic–Plastic–Hydro constitutive relation; this approach was also taken by Lopez-Puente et al. [26] to numerically study the effect of adhesive layer thickness on the ballistic limit velocity of ceramic/metal armors.

The material parameters used in the J–C model and the Mie-Gruneisen equation of state model for AISI 304 stainless steel are summarized in Table 1 [27,28], those for AD 98 alumina used in the JH-2 model are presented in Table 2 [25], and the main material constants of the epoxy resin are: mass density 1185 kg/m^3, shear modulus 769 MPa, yield stress 70 MPa.

4. Experimental validation

To check the accuracy of the present FE stimulations, sandwich plates with three types of hybrid core as shown in Fig. 1 and geometrical dimensions as indicated in Fig. 2 are fabricated and a series of experimental measurements are subsequently carried out.

4.1. Test samples

The procedures employed to fabricate the composite lattice truss-cored sandwiches of Fig. 1 are similar to those described in Yungwirth et al. [18] and hence not repeated here. The pyramidal lattice trusses are firstly made from 1.9 mm thick sheet of stainless steel (AISI 304) using the method of sheet slitting, expansion and flattening, which are then bonded to 1.5 mm thick AISI 304 stainless steel face-sheets with the transient liquid phase bonding process. The as-fabricated lattice truss members have square cross-sections (1.9 mm × 1.9 mm). To fabricate a Type III structure with pyramidal lattice-ceramic-epoxy core, epoxy resin is firstly poured into the pyramidal lattice core of Type I structure which is properly sealed at its edges to prevent epoxy leakage. Subsequently, as ceramic prisms are inserted into the epoxy-filled lattice core, excessive epoxy spills out of the core to ensure the remaining epoxy can adequately fill the void space between the pyramidal lattice and the ceramic prisms. The ceramic prism inserts are made of AD 98 alumina rods. The hemispherical nosed projectile, diameter 6 mm and length 15 mm (Fig. 2), is made from stainless steel (AISI 304). Note that these samples with selected geometrical dimensions are used mainly to obtain experimental results that can be used to check the validity of numerical simulations. In subsequent numerical studies, the structural and topological parameters will be systematically varied to explore their influence upon the ballistic behavior of hybrid-cored sandwiches.

4.2. Experimental measurements

Fig. 4 illustrates schematically the experimental setup, with a ballistic rifle used to launch the impact projectile. To remove possible source of variability in the measurements, the rifle is sighted carefully so that the projectile can impact right at the apex of the pyramidal trusses connected to the front face-sheet, which is also the center of the sandwich plate (Fig. 2). A pair of brake screens spaced 300 mm apart and connected to a timing device is used to measure the projectile entry velocity. This is achieved by evaluating the ratio of screen spacing divided by the time difference between the moments separately triggered by the projectile impacting the first and second screens. In view of the drift effect in the process of projectile penetration through the sandwich, X-ray tomography is adopted to measure the exit velocity of the projectile. In a separate scheme, the exit velocity of the projectile is determined by evaluating the ratio of the distance between two projectile shadows in the X-ray native divided by the time difference between the two triggers.

4.3. Comparison with experimental measurements

Fig. 5 compares the experimental results with the FE simulation results for the three sandwich types considered in the present study. Whilst Fig. 5a plots the projectile exit velocity as a function

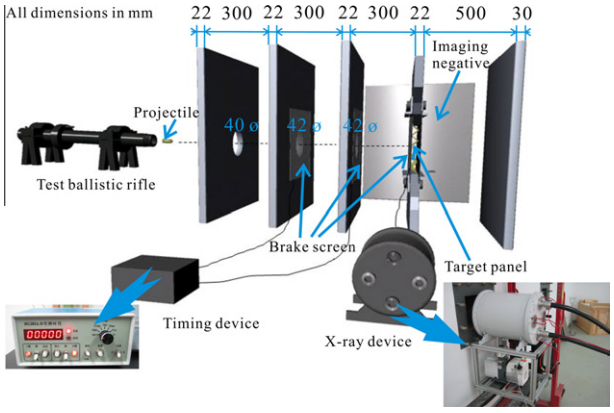

Fig. 4. Experimental setup for measuring ballistic response of hybrid-cored sandwich plate.

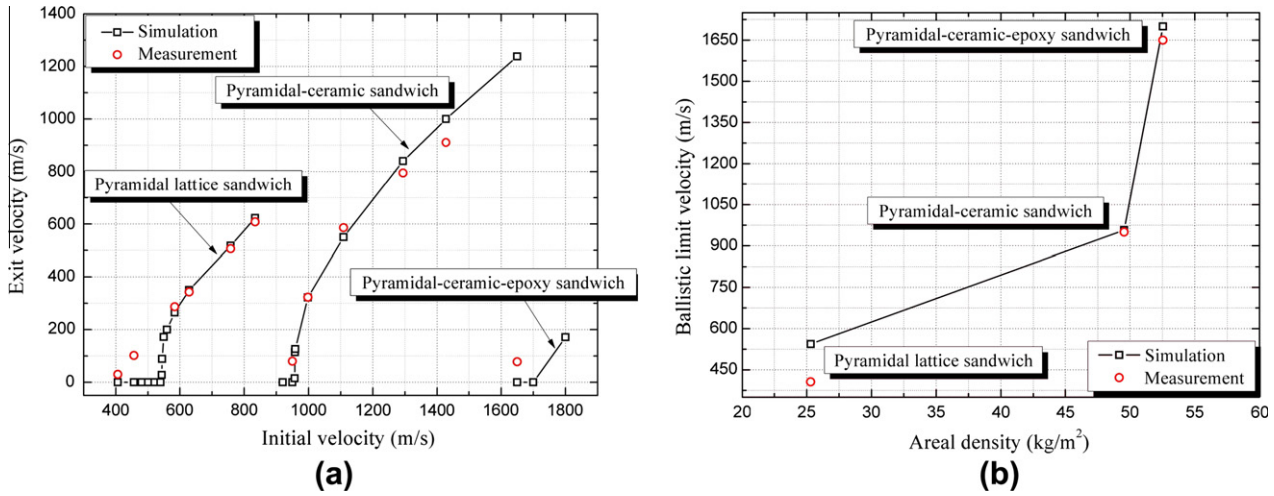

Fig. 5. (a) Projectile exit velocity plotted as a function of initial impact velocity and (b) ballistic limit velocity plotted as a function of sandwich areal density for three different hybrid-cored sandwich plates.

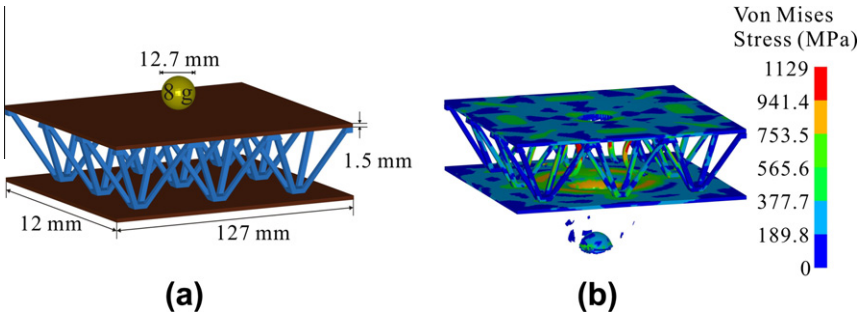

Fig. 6. All metallic pyramidal truss-cored sandwich plate (Type I) impacted by spherical projectile made of plain carbon steel: (a) finite element model; and (b) predicted penetration process of projectile and distribution of Mises stress.

of its initial velocity impacting the sandwich plate, Fig. 5b plots the ballistic limit velocity as a function of the areal density of the sandwich. Overall, good agreement is achieved for each type of the sandwich, demonstrating the feasibility of using FE simulations to investigate the ballistic performance of hybrid-cored sandwich structures.

The results of Fig. 5 show that inserting ceramic prisms alone into the empty lattice core results in about 100% increase of the ballistic limit velocity, and the ballistic limit velocity is increased by about 280% if the insertion is combined with epoxy bonding. This increase in ballistic limit velocity is however accompanied by an increase in sandwich areal density by about 100% and 130%, respectively. These results indicate that by integrating the ceramic insertions, the pyramidal metallic lattice trusses and the metallic face-sheets as a whole using the infiltrated epoxy, the ballistic resistance of the sandwich plate can be significantly enhanced, with a moderate increase in its areal density. More detailed analysis for the ballistic responses of the sandwich is elucidated in subsequent sections.

For further validation, the experimental results of Yungwirth et al. [17] for empty pyramidal lattice-truss cored sandwich plates (without ceramic insertions and epoxy resin bonding, Type I) are compared with the present FE predictions. As illustrated in Fig. 6, the fully-clamped sandwich plate made of AISI 304 stainless steel is penetrated by a spherical projectile made of plain carbon steel. The geometrical dimensions of the sandwich plate and the projectile as well as experimental details can be found in Yungwirth et al. [17].

At the initial impact velocity of 1206 m/s, whilst Fig. 6a presents the full scale FE model for the simulation, Fig. 6b shows the predicted spreading of stress waves in the sandwich structure and the penetration process of the projectile. Fig. 7 compares the numerically predicted exit velocity of the projectile with that measured [17] for selected initial impact velocities. Again, close agreement between simulation and measurement is achieved. Further, as shown in Fig. 8, the simulated failure modes (e.g., perforation,

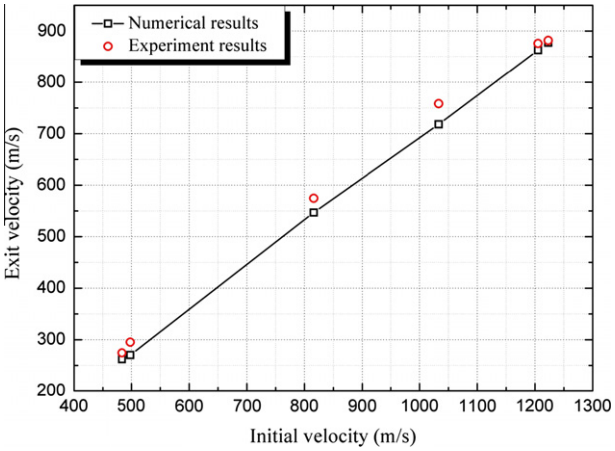

Fig. 7. Finite element simulation results compared with experimental measurements [17] for empty pyramidal lattice truss-cored sandwich plate (Type I) impacted by spherical projectile (Fig. 6).

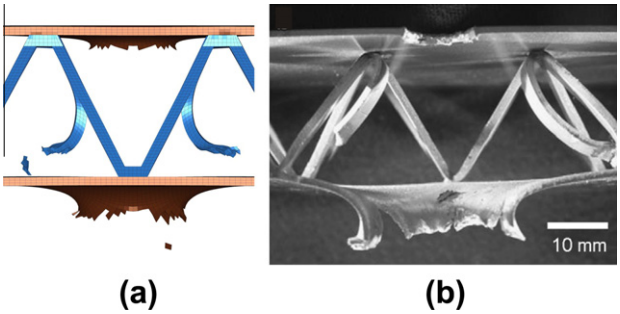

Fig. 8. Comparison of numerically predicted and experimental measured [17] local damage of all metallic pyramidal lattice truss-cored sandwich plate (Type I) after penetration with spherical projectile.

plastic bending, fracturing/tearing) of the pyramidal lattice truss-cored sandwich structure resembles that observed in the experiment [17], demonstrating the capability of the FE approach adopted in the present study.

5. Results and discussion

The experimentally-validated FE model is employed in this section to explore more details concerning the ballistic performance of the three types of hybrid-cored sandwich plate as shown in Fig. 1. Unless otherwise stated, the simulation parameters are identical to those described in the preceding sections.

5.1. Sandwich plate with empty pyramidal lattice truss core (Type I)

Under the conditions as specified in the present study, the simulation results show that a sandwich plate with empty pyramidal lattice core (Type I) cannot be fully penetrated by the projectile if its entry velocity is less than 544 m/s, i.e., the ballistic limit velocity of the sandwich plate is 544 m/s when the projectile impacts the plate at its center (Fig. 2). At the ballistic limit velocity, Fig. 9a plots the energy absorbed by each sub-structure of the plate as a function of penetration time, with the corresponding failure modes presented in Fig. 9b. As the projectile trajectory is often altered by the face-sheets and the core, Fig. 10 plots the velocity of the projectile perpendicular to the sandwich plate (i.e., *Z*-velocity) as a function of penetration time, which is also compared with those of other sandwich types considered in the present study. Note that, whilst the black curve in Fig. 10 represents that of the projectile launched at the initial ballistic limit velocity of 544 m/s for Type I sandwiches, the remaining curves in Fig. 10 are obtained with the initial projectile velocity of 1700 m/s for sandwiches with alternative topologies as well as monolithic plates.

For Type I structures, it is seen from Fig. 10 (black curve) that the velocity of the projectile sharply drops while penetrating through either the front or back face-sheet, during the period of 0–16 μs and 46–80 μs, respectively. At 12 μs, the energy absorbed by the front face-sheet reaches a peak (Fig. 9a) due mainly to localized plastic deformation perforation fracture (Fig. 9b).

The pyramidal lattice core absorbs the impact energy mainly by large bending deflections of the truss members and fracturing at the vertices of the connecting joints (Fig. 9b). The truss members of the central unit begin to crack at 44 μs and become fully fractured at 58 μs corresponding to the inflexion point on the curve of Fig. 9a.

The back face-sheet absorbs considerably more energy than the front face sheet (Fig. 9a). The projectile penetrates through the front face-sheet within 12 μs, leading mainly to perforation fracture. At this point, the pyramidal lattice core is still intact and hence can still provide support for the front face-sheet to resist its bending deformation (Fig. 9b). Whereas, the projectile that has been slowed down by both the front face-sheet and the lattice truss members penetrates through the back face-sheet over a much longer time period, inducing not only perforation fracture but also large plastic deformation of the back face-sheet (Fig. 9b) because the lattice core has now been much weakened due to severe damage in the central impact regime. At 72 μs the energy absorbed by the back face-sheet becomes steady (Fig. 9a).

5.2. Sandwich plate with pyramidal lattice-ceramic core (Type II)

The ballistic resistance of sandwich plates with pyramidal lattice-ceramic core (Type II) is examined next, with 1700 m/s selected as the entry velocity of the projectile impacting the sandwich at its center (Fig. 2). The exit velocity of the projectile, deformation/failure pattern, and energy absorption capacity of each sub-structure are concerned. Note that 950 m/s, not 1700 m/s, is the ballistic limit velocity of Type II sandwich plates (Fig. 5).

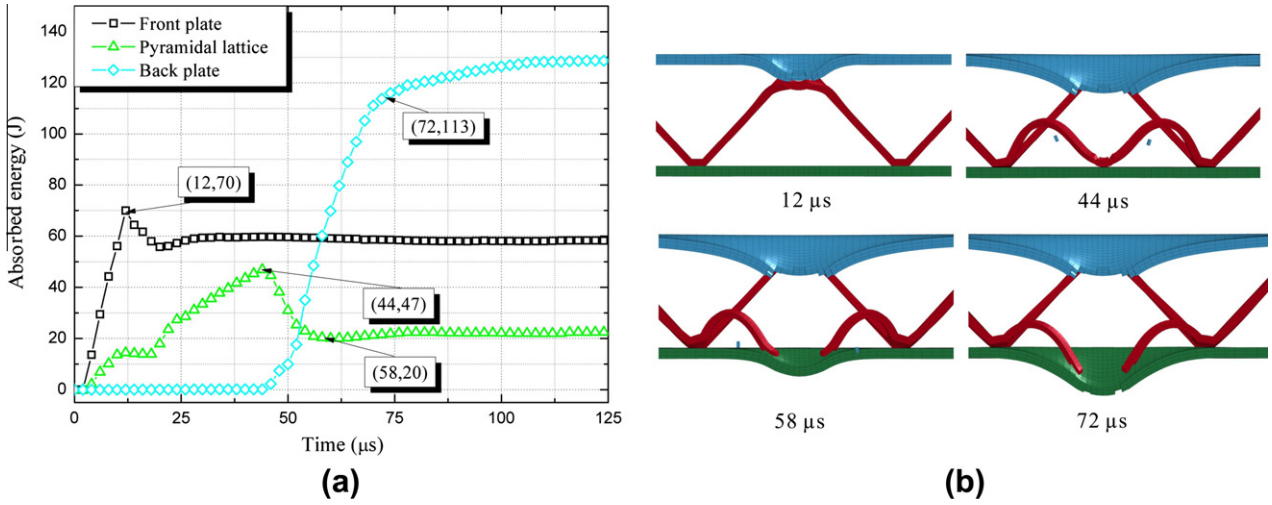

Fig. 9. (a) Energy absorption by each sub-structure plotted as a function of impact time and (b) failure modes of sub-structures for sandwich plate with empty pyramidal lattice core (Type I) at initial impact velocity of 544 m/s.

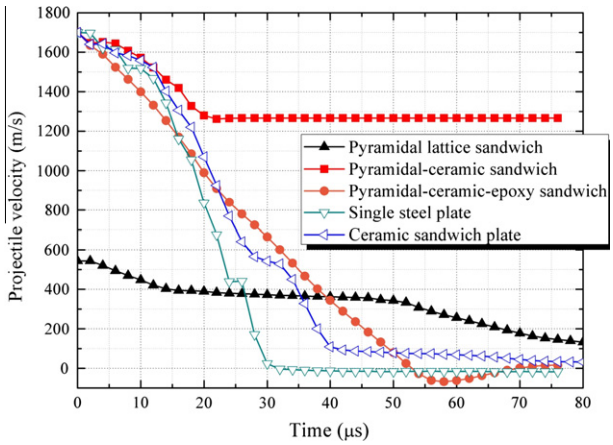

Fig. 10. *Z*-velocity of hemispherical projectile plotted as a function of time at initial impact velocity of 544 m/s for sandwich plate with empty pyramidal lattice core (Type I), 1700 m/s for sandwich plate with pyramidal-ceramic hybrid core (Type II), sandwich plate with pyramidal-ceramic-epoxy hybrid core (Type III), 14.9 mm thick single steel plate, and ceramic-cored sandwich plate (front/back face sheet: 1.5 mm thick AISI 304 stainless steel; homogeneous ceramic core: 18 mm thick).

The results presented in Fig. 10 show that the velocity of the projectile sharply slows down during the period of 6–20 μs, due mainly to the superior ballistic resistance of the central ceramic prism. As the projectile penetrates across the sandwich, it is continuously cut and eroded by the ceramic prism (Fig. 11a). However, whilst the ceramic insertions reduce the velocity, mass and kinetic energy of the projectile, the sandwich plate cannot defend the projectile at the velocity of 1700 m/s. Since the ceramic prisms are freely inserted into the lattice core, the stress waves generated in the central impact zone cannot spread to the perimeter ceramic prisms effectively. Therefore, the ballistic resistance of the sandwich is mainly contributed by the central ceramic prism directly under impact, with the energy absorption capability of the remaining ceramic prisms not fully exploited; see Figs. 11 and 12b later. Although its ballistic limit velocity is considerably larger than that of Type I sandwich, this is compromised by considerable increase in total mass, as previously discussed.

5.3. Sandwich plate with pyramidal lattice-ceramic-epoxy core (Type III)

To simulate the dynamic response and ballistic resistance of sandwich plates having pyramidal lattice-ceramic-epoxy hybrid core (Type III), the initial impact velocity of 1700 m/s is selected since the projectile at this speed can just not perforate the structure, i.e., it is the ballistic limit velocity of this sandwich type (Fig. 2). The sandwich plate is composed of two parallel face-sheets connected by pyramidal lattice core with inserted ceramic prisms, with epoxy resin providing the bonding between the truss members, the face-sheets and the ceramic prisms. As a result, when the projectile penetrates across the sandwich, whilst the ceramic prisms slow down the projectile, the stress wave spreads from the central impact zone to the whole structure due to the bonding effects of epoxy resin. Towards the end of the penetration, the projectile is severely eroded by the central ceramic insertion (Fig. 11b), similar to that observed for the case of Type II (Fig. 11a). Further, at about 8 μs, the interface between the epoxy resin layer and the back face sheet cracks and even separates (Fig. 11b), agreeing well with that observed during the present experiment.

From the viewpoint of ballistic resistance and energy absorption, the numerical and experimental results presented here demonstrate that sandwich plates with pyramidal lattice-ceramic-epoxy hybrid cores (Type III) outperform the two other sandwich types (Types I and II). This is because the epoxy resin is capable of ensuring the integrity of the sandwich, thus there is significant spreading of stress waves in the structure, leading to a more smooth projectile velocity curve than that of Type II sandwich (Fig. 10). Correspondingly, apart from the central ceramic prism, the side prisms also fracture as a result of projectile penetration, which is not observed in Fig. 11a for Type II. Also, as shown in Fig. 11b, even though the ceramic prisms fracture into small fragments, these are constrained by the epoxy resin (not shown directly in Fig. 11b for clarity), providing further resistance to projectile penetration. Further, due to epoxy bonding effects, the lattice truss members directly under impact deflect much less (Fig. 11b) in comparison with those in sandwiches without void-filling epoxy (Figs. 9b and 11a).

For comparison, the dynamic responses and ballistic resistance of a single AISI 304 stainless steel plate and a ceramic-cored

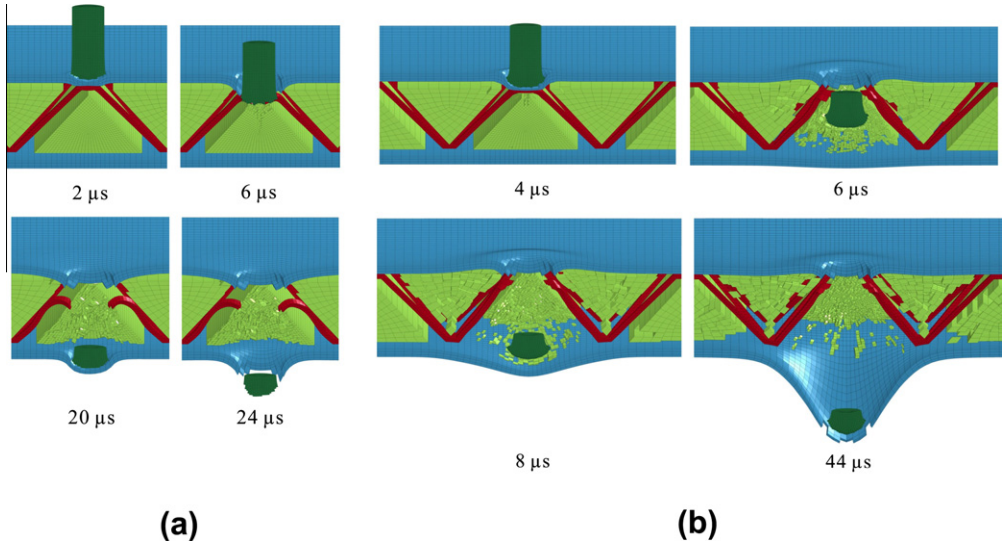

Fig. 11. (a) Evolution of deformation and failure in sandwich plate with pyramidal lattice-ceramic core (Type II) at initial impact velocity of 1700 m/s, and (b) failure mode of sandwich plate with pyramidal lattice-ceramic-epoxy core (Type III) at initial impact velocity of 1700 m/s (Euler elements for epoxy resin marked for clarity).

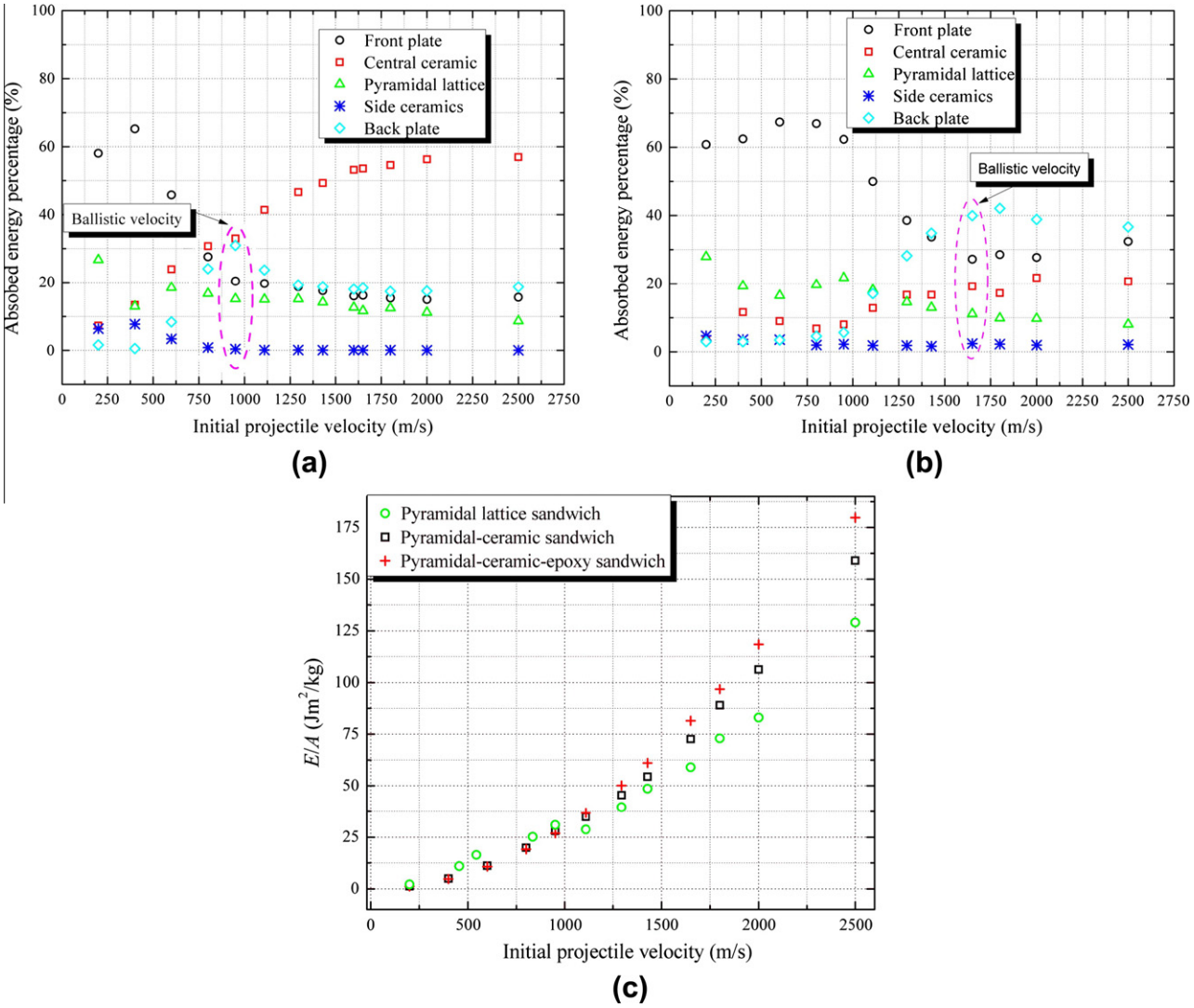

Fig. 12. Energy absorption percentage of each sub-structure in sandwich plate with (a) pyramidal lattice-ceramic core (Type II) and (b) pyramidal lattice-ceramic-epoxy core (Type III); and (c) absorbed total energy normalized by areal density of each sandwich type for selected initial projectile velocities.

sandwich plate are simulated, and the results are presented in Fig. 10 together with those for hybrid-cored sandwich plates. Under the present simulation conditions, it is seen from Fig. 10 that a 14.9 mm thick single steel plate and a sandwich plate with 1.5 mm thick front/back AISI 304 stainless steel face sheet and 18 mm thick homogenous ceramic core have the same penetration resistance as that of the sandwich with pyramidal lattice-ceramic-epoxy hybrid core (Type III), i.e., 1700 m/s. However, the hybrid-cored sandwich plate achieves this feat at only 40% and 63% weight of the single steel plate and the ceramic-cored sandwich plate, respectively. In other words, the pyramidal-ceramic-epoxy hybrid core can efficiently prolong the penetration period of the projectile, and hence ensure each sub-structure can deform and absorb the impact energy sufficiently. This is elucidated further below.

5.4. Energy absorption by sub-structures of hybrid-cored sandwich plates

Sandwich plates with pyramidal-ceramic and pyramidal-ceramic-epoxy cores penetrated by hemispherical projectile at different initial impact velocities are simulated to explore the energy absorption capability of each sub-structure. The results are separately presented in Fig. 12a and b in terms of absorption percentage of the total impact energy.

For sandwich plates with pyramidal-ceramic hybrid core (Type II), it is seen from Fig. 12a that the front face-sheet plays a dominant role in energy absorption when the impact velocity is below the ballistic limit velocity. As the velocity is increased, the percentage of energy absorbed by the central ceramic prism becomes increasingly more significant, overtaking that by the front face-sheet when the ballistic limit velocity is reached; simultaneously, the energy absorbed by the back face-sheet also exceeds that by the front face-sheet (Fig. 12a). As the velocity just exceeds the ballistic limit velocity, plastic deformation peaks in the back face-sheet and hence its absorbed energy percentage also peaks. However, the energy absorbed by the central ceramic prism continues to rise even beyond the ballistic limit velocity, accounting for about 60% of the total impact energy. In other words, the central ceramic prism plays a dominant role when the initial impact velocity exceeds the ballistic limit velocity.

For sandwich plates with pyramidal-ceramic-epoxy hybrid core (Type III), Fig. 12b shows that either the front face-sheet or the back face-sheet absorbs more energy than the other sub-structures including the central ceramic prism, except in the low velocity regime. Due to epoxy bonding effects, the front and back face-sheets

absorb the projectile energy through not only local perforation fracture but also, more importantly, plastic deformation beyond the central impact zone. Contrast to the case without epoxy resin (Fig. 12a), the back face-sheet now plays a leading role near and beyond the ballistic limit velocity. At the same time, the central ceramic prism also absorbs a considerable amount of impact energy.

For both types of hybrid-cored sandwich, as the initial impact velocity exceeds 2000 m/s, the energy absorbed by each substructure tends to remain unchanged, as shown in Fig. 12a–b. Fig. 12c plots the total energy absorption normalized by the areal density of each sandwich type as a function of initial projectile velocity. For projectile velocities below about 1000 m/s, Type I structure is more efficient than Types II and III because of its low areal density. As the velocity is increased, the superiority of Type III over the other two sandwich types is clearly established.

5.5. Eroding effects of hybrid-cored sandwich plate on penetrating projectile

To explore further the mechanisms underlying the elevated ballistic limit velocities of Type II and III sandwich plates relative to that of Type I sandwiches, Fig. 13 plots the relative mass and shape of the projectile as it exits the sandwich as functions of the initial impact velocity. The relative mass of the projectile is defined here as the ratio of its residual mass to initial mass.

For both Type II and III sandwiches, the projectile relative mass decreases monotonically with increasing initial impact velocity, accompanied by significant erosion of the projectile. For Type II sandwiches, as the initial impact velocity exceeds the ballistic limit velocity, there exists obvious deflection of the projectile upon penetrating across the sandwich; see Fig. 13a. This may be attributed to the discrete nature of this sandwich type without epoxy resin bonding, which becomes unstable when subjected to relatively intense impact loading, causing the penetrating projectile to deviate from its ballistic trajectory. In contrast, such deflection of the projectile is absent in Type III sandwiches (Fig. 13b), as structural integrity is ensured by epoxy resin. Further, by comparing Fig. 13a with b, it can be seen that the projectile exiting Type III sandwiches is more square and dumpy than that exiting Type II sandwiches, again due to the constraining effects of ceramic-epoxy system, resulting in enhanced ballistic performance.

5.6. Maximum displacement of hybrid-cored sandwich plate

Fig. 14 plots the maximum z-displacement of the back face-sheet normalized to its thickness as a function of the initial impact velocity for both Type II and III sandwich plates as the projectile penetrates across the sandwich. For both sandwich types, the back face-sheet displacement increases as the impact velocity is increased, peaking when the ballistic limit velocity is reached and then decreases. For Type III, however, the decrease after reaching the ballistic limit velocity is relatively small and, as the impact velocity is further increased, the back face-sheet displacement starts to increase again (Fig. 14b). This is attributed to the integrated hybrid-core structure of Type III sandwich, enabling the back face-sheet to absorb considerable amount of total impact energy through local plastic deformation and shear tearing even after the ballistic limit velocity is reached. As a result, its protuberance after projectile penetration is more significant than that of Type II without using void-filling epoxy resin (Fig. 14a).

5.7. Influence of face sheet thickness on ballistic resistance of hybrid-cored sandwich

A preliminary optimal design toward maximum ballistic resistance is conducted in this section. Since the sandwich plate with pyramidal-ceramic-epoxy hybrid core (Type III) displays superior ballistic resistance relative to other sandwich types, it is further optimized in terms of face-sheet thickness. To this end, four combinations of the front and back face-sheet thicknesses, i.e., (0.5–2.5 mm), (1–2 mm), (2–1 mm), and (2.5–0.5 mm), are compared with the reference combination, (1.5–1.5 mm), and the ballistic limit velocity of each combination is calculated. As the face-sheet thickness is varied, the pyramidal-ceramic-epoxy hybrid core remains unchanged and hence the total mass of the sandwich is fixed for the comparison. The results are summarized in Fig. 15. Note that, in Fig. 15, the face-sheet configurations (1/6–5/6), (1/3–2/3), (1/2–1/2), (2/3–1/3) and (5/6–1/6) correspond to the face-sheet thickness arrangements of (0.5–2.5 mm), (1–2 mm), (1.5–1.5 mm), (2–1 mm) and (2.5–0.5 mm), respectively.

The results of Fig. 15 demonstrate that the ballistic limit velocity of Type III sandwich depends significantly upon the arrangement of face-sheets having different thicknesses, and the highest ballistic limit velocity (2200 m/s) is attained by the (1/6–5/6)

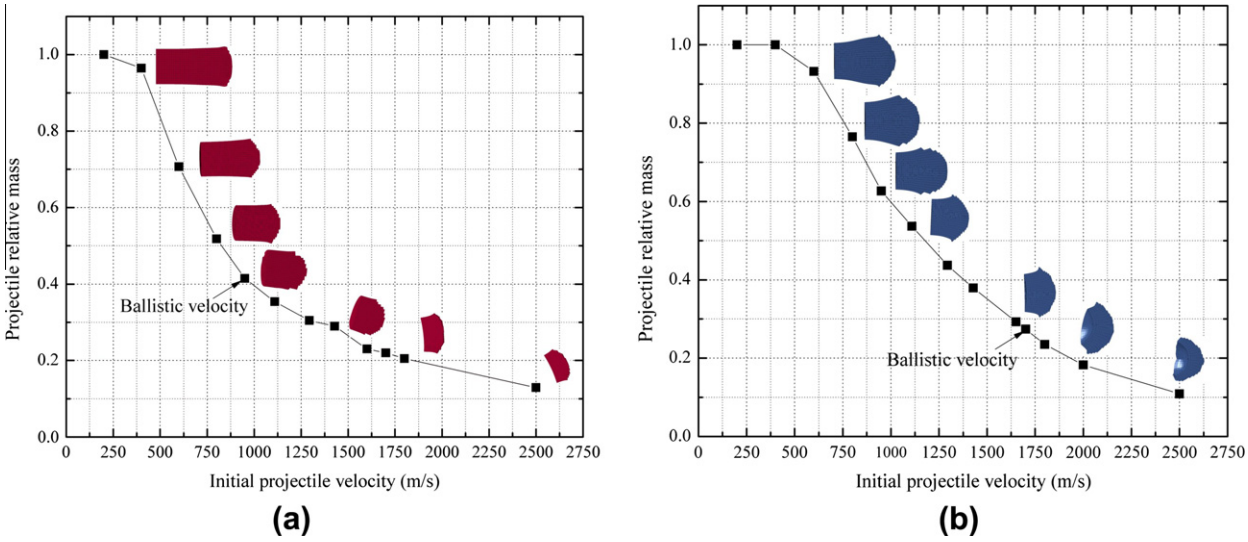

Fig. 13. Relative mass and residual shape of projectile exiting the sandwich plotted as functions of initial impact velocities for (a) pyramidal lattice-ceramic core (Type II) and (b) pyramidal lattice-ceramic-epoxy core (Type III).

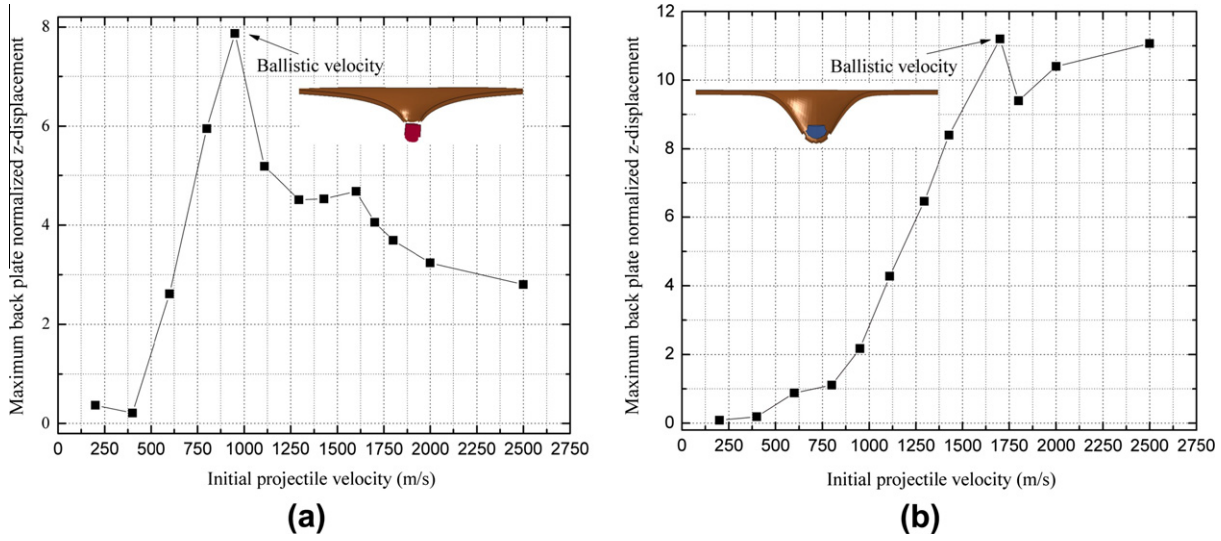

Fig. 14. Maximum normalized z-displacement of back face-sheet plotted as a function of initial impact velocity for sandwich plate with (a) pyramidal lattice-ceramic core (Type II) and (b) pyramidal lattice-ceramic-epoxy core (Type III).

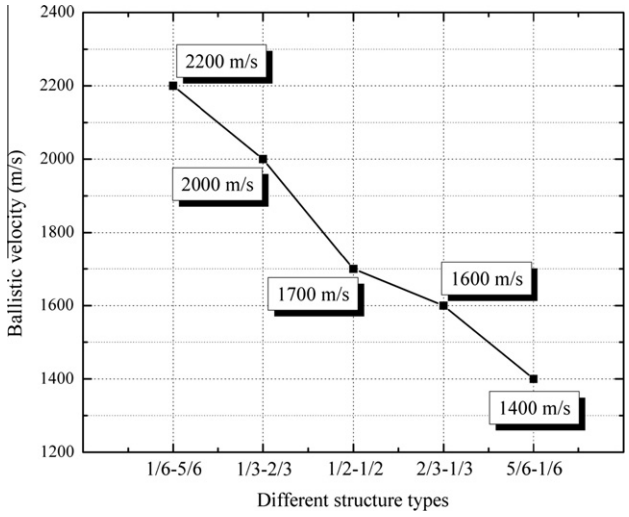

Fig. 15. Ballistic limit velocity of Type III sandwich structure for five different arrangements of face-sheet thicknesses.

configuration amongst the five configurations considered. As the thickness of the front face-sheet is reduced, the ballistic limit velocity increases monotonically from 1400 m/s for configuration (5/6–1/6) to 2200 m/s for configuration (1/6–5/6). Consequently, with the total mass of the sandwich structure fixed, decreasing the thickness of the front face-sheet whilst increasing that of the back face-sheet leads to enhanced energy absorption and ballistic limit velocity.

Fig. 16a presents the absorbed total energy for each configuration at its ballistic limit velocity. It is seen that the (1/6–5/6) configuration, i.e., sandwich with the thinnest front face-sheet and thickest back face-sheet, has the best energy absorption performance, which is consistent with the fact that this configuration also corresponds to the highest ballistic limit velocity (Fig. 15). To explore the mechanisms underlying the effect of face-sheet thickness upon the ballistic limit velocity as displayed in Fig. 15. Fig. 16b presents the absorbed energy percentage of each sub-structure at the ballistic limit velocity for each configuration. It can be observed from Fig. 16b that the energy absorbed by the back face-sheet in (1/6–5/6), (1/3–2/3), and (1/2–1/2) configurations possess larger portions than those in (2/3–1/3) and (5/6–1/6),

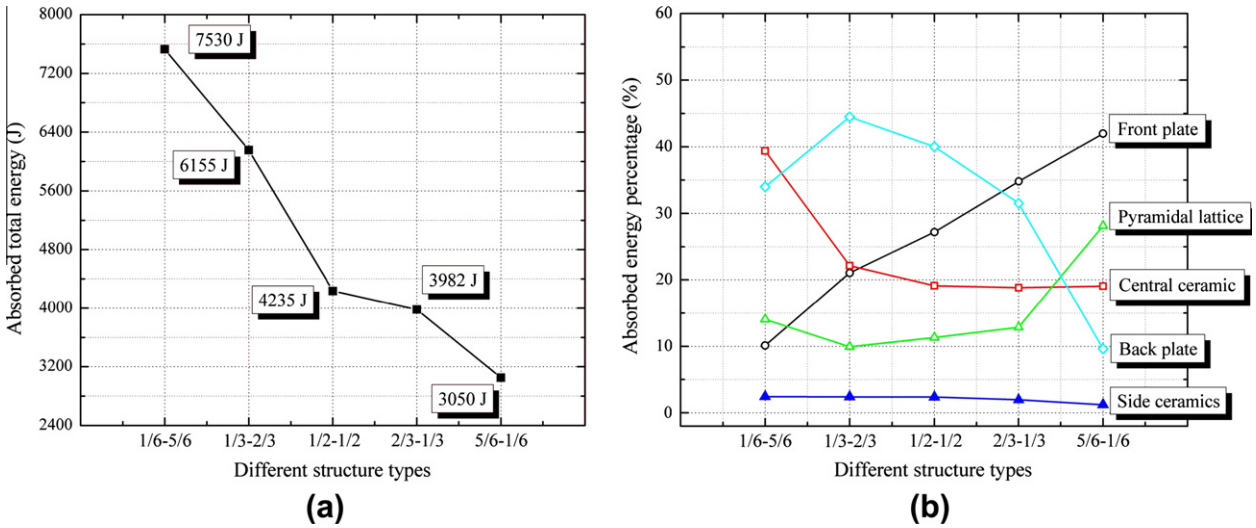

Fig. 16. (a) Absorbed total energy and (b) energy percentage of each sub-structure for five different arrangements of face-sheet thicknesses at their corresponding ballistic limit velocities.

leading to increased ballistic limit velocity. Though the latter have thicker front face-sheets, the interaction time between the projectile and the front face-sheet is relatively short due to the initially high impact velocity of the projectile. At this stage, the front face-sheet absorbs the impact energy mainly by localized shearing deformation and perforation fracture, as the integrated hybrid core can provide sufficient support for it to resist large scale bending deformation. Once the penetrating process is complete across the front face-sheet, the projectile is considerably slowed down by the pyramidal-ceramic-epoxy hybrid core before reaching the back face-sheet. Since the hybrid core is considerably damaged during this stage, the bending/shearing deformation regime in the back face-sheet is considerably broadened in comparison with that in the front face-sheet. Further, as the front face-sheet thickness is reduced (correspondingly, the back face-sheet thickness is increased due to the constraint of equal mass), the role of the central ceramic prism increases, peaking when the front face-sheet becomes the thinnest. Consequently, it may be inferred from Figs. 15 and 16 that a combination of enhanced energy absorption by both the back face-sheet and the central ceramic prism causes the ballistic limit velocity to increase with decreasing front face-sheet thickness and increasing back face-sheet thickness. Further, it is interesting to see that the energy percentage absorbed by the side ceramic prisms is relatively small and nearly independent of the face-sheet thickness (Fig. 16b).

6. Concluding remarks

A combined theoretical and experimental study on the energy absorption and ballistic performance of fully-clamped lightweight sandwich plates with three different types of core has been carried out, including pyramidal lattice core, pyramidal-ceramic hybrid core and pyramidal-ceramic-epoxy hybrid core. The following conclusions are drawn.

The projectile kinetic energy is absorbed mainly through the plastic deformation and shear expansion of the face-sheets, the fracture damage of the solidified epoxy resin and ceramic prisms, as well as the macroscopically bending deformation of the whole structure. The high-strength/hardness ceramic prisms inserted in the pyramidal core can significantly enhance the ballistic resistance of the structure, resulting from the drastic erosion effects of the ceramic prism on the ballistic projectile. The infiltrated epoxy resin adheres all the sub-structures as an integrated whole, thus appreciably improving the ballistic energy absorption capacity of the whole structure. Therefore, sandwich plates with pyramidal-ceramic-epoxy hybrid core possess superior ballistic resistance and energy absorption capability over those without ceramic inserted or epoxy infiltrated. In addition, it is demonstrated that the back face-sheet plays a more significant role than the front face-sheet in resisting ballistic impacts. When the total mass of the sandwich plate is fixed, decreasing the thickness of the front face-sheet whilst increasing that of the back face-sheet leads to enhanced energy absorption and ballistic limit velocity.

Acknowledgments

This work is supported partially by the National Basic Research Program of China (2011CB6103005), the National Natural Science Foundation of China (11072188, 11102148, 10825210 and 51002114) and the Fundamental Research Funds for Central Universities.

References

[1] Ashby MF, Evans AG, Fleck NA, Gibson LJ, Hutchinson JW, Wadley HNG. Metal foam: a design guide. London: Butterworth–Heinemann; 2000.
[2] Banhart J, Ashby MF, Fleck NA. Metal foams and porous metal structures. In: 1st International conference on metal foams and porous metal structures. Bremen (Germany): MIT; 1999.
[3] Evans AG, Hutchinson JW, Ashby MF. Multifunctionality of cellular metal systems. Prog Mater Sci 1998;43(3):171–221.
[4] Gibson LJ, Ashby MF. Cellular solids: structure and properties. second ed. Cambridge: Cambridge University Press; 1997.
[5] Wadley HNG, Fleck NA, Evans AG. Fabrication and structural performance of periodic cellular metal sandwich structures. Compos Sci Technol 2003;63(16):2331–43.
[6] Xin FX, Lu TJ. Sound radiation of orthogonally rib-stiffened sandwich structures with cavity absorption. Compos Sci Technol 2010;70(15):2198–206.
[7] Xin FX, Lu TJ. Analytical modeling of fluid loaded orthogonally rib-stiffened sandwich structures: sound transmission. J Mech Phys Solids 2010;58(9):1374–96.
[8] Arias A, Rodríguez-Martínez JA, Rusinek A. Numerical simulations of impact behaviour of thin steel plates subjected to cylindrical, conical and hemispherical non-deformable projectiles. Eng Fract Mech 2008;75(6):1635–56.
[9] Børvik T, Clausen AH, Hopperstad OS, Langseth M. Perforation of AA5083-H116 aluminium plates with conical-nose steel projectiles – experimental study. Int J Impact Eng 2004;30(4):367–84.
[10] Børvik T, Hopperstad OS, Berstad T, Langseth M. Perforation of 12 mm thick steel plates by 20 mm diameter projectiles with flat, hemispherical and conical noses: Part II: numerical simulations. Int J Impact Eng 2002;27(1):37–64.
[11] Børvik T, Langseth M, Hopperstad OS, Malo KA. Perforation of 12 mm thick steel plates by 20 mm diameter projectiles with flat, hemispherical and conical noses: Part I: experimental study. Int J Impact Eng 2002;27(1):1–35.
[12] Børvik T, Leinum JR, Solberg JK, Hopperstad OS, Langseth M. Observations on shear plug formation in Weldox 460 E steel plates impacted by blunt-nosed projectiles. Int J Impact Eng 2001;25(6):553–72.
[13] Teng X, Wierzbicki T, Huang M. Ballistic resistance of double-layered armor plates. Int J Impact Eng 2008;35(8):870–84.
[14] Radford DD, Deshpande VS, Fleck NA. The use of metal foam projectiles to simulate shock loading on a structure. Int J Impact Eng 2005;31(9):1152–71.
[15] Rathbun HJ, Zok FW, Waltner SA, Mercer C, Evans AG, Queheillalt DT, et al. Structural performance of metallic sandwich beams with hollow truss cores. Acta Mater 2006;54(20):5509–18.
[16] Tian YS, Lu TJ. Optimal design of compression corrugated panels. Thin-Walled Struct 2005;43(3):477–98.
[17] Yungwirth CJ, Wadley HNG, O'Connor JH, Zakraysek AJ, Deshpande VS. Impact response of sandwich plates with a pyramidal lattice core. Int J Impact Eng 2008;35(8):920–36.
[18] Yungwirth CJ, Radford DD, Aronson M, Wadley HNG. Experiment assessment of the ballistic response of composite pyramidal lattice truss structures. Compos Part B – Eng 2008;39(3):556–69.
[19] Krishnan K, Sockalingam S, Bansal S, Rajan SD. Numerical simulation of ceramic composite armor subjected to ballistic impact. Compos Part B – Eng 2010;41(8):583–93.
[20] Smojver I, Ivancevic D. Bird strike damage analysis in aircraft structures using Abaqus/explicit and coupled Eulerian Lagrangian approach. Compos Sci Technol 2011;71(4):489–98.
[21] Yadav S, Ravichandran G. Penetration resistance of laminated ceramic/polymer structures. Int J Impact Eng 2003;28(5):557–74.
[22] Zaera R, Sánchez-Sáez S, Pérez-Castellanos JL, Navarro C. Modelling of the adhesive layer in mixed ceramic/metal armours subjected to impact. Compos Part A – Appl S 2000;31(8):823–33.
[23] Livermore Software Technology Corporation, California, USA, LS-DYNA 970; 2005.
[24] Johnson GR, Holmquist TJ. Shock wave and high strain rates and high pressures. New York: Marcel Dekker Inc; 1992.
[25] McIntosh G. The Johnson–Holmquist ceramic model as used in LS-DYNA 2d. Quebec, Canada: Report of Canada National Defence; 1998.
[26] Lopez-Puente J, Arias A, Zaera R, Navarro C. The effect of the thickness of the adhesive layer on the ballistic limit of ceramic/metal armours: an experimental and numerical study. Int J Impact Eng 2005;32(1):321–36.
[27] Mori LF, Lee S, Xue ZY, Vaziri A, Queheillalt DT, Dharmasena KP, et al. Deformation and frcture modes of sandwich structures subjected to underwater impulsive loads. J Mech Mater Struct 2007;2(10):1981–2006.
[28] Centrury Dynamics Ltd., Dynamic House, Hurst Road, Horsam, West Sussex, England, AUTODYN-2D; 1998.